EUROPEAN FUSION DEVELOPMENT AGREEMENT

EFDA–JET–PR(05)42

T. Tala, F. Imbeaux, V.V. Parail, C. Bourdelle, G. Corrigan, X. Garbet, D.J. Heading, X. Litaudon, P.I. Strand, J. Weiland and JET EFDA contributors

Fully Predictive Time-Dependent Transport Simulations of ITB Plasmas in JET, JT-60U and DIII-D

Fully Predictive Time-Dependent Transport Simulations of ITB Plasmas in JET, JT-60U and DIII-D

T. Tala[1], F. Imbeaux[2], V.V. Parail[3], C. Bourdelle[2], G. Corrigan[3], X. Garbet[2], D.J. Heading[3], X. Litaudon[2], P.I. Strand[4], J. Weiland[4] and JET EFDA contributors*

[1]Association Euratom-Tekes, VTT Processes, P.O. Box 1608, FIN-02044 VTT, Finland
[2]Association Euratom-CEA, CEA-DSM-DRFC Cadarache, 13108, St Paul lez Durance, France
[3]EURATOM/UKAEA Fusion Association, Culham Science Centre, Abingdon, OX14 3DB, UK
[4]Association Euratom-VR, Chalmers University of Technology, Gothenburg, Sweden
** See annex of J. Pamela et al, "Overview of JET Results ",*
(Proc. 20th IAEA Fusion Energy Conference, Vilamoura, Portugal (2004).

Preprint of Paper to be submitted for publication in
Nuclear Fusion

ABSTRACT

For the first time, the predictive capabilities of the mixed Bohm/GyroBohm, Weiland and 'retuned' GLF23 transport models are investigated with ITB discharges from the ITPA ITB database with fully predictive, time-dependent transport simulations. A range of plasma conditions is examined for JET, JT-60U and DIII-D discharges with ITBs. The simulations show that the Bohm/GyroBohm model is able to follow the time evolution of the discharge from the preheating phase without an ITB through the ITB onset phase until the high performance phase within a fair accuracy in most cases in JET and JT-60U. This indicates the importance of the interplay between the magnetic shear and $\omega_{E\times B}$ flow shear in ITB formation since these are the mechanisms that govern the ITB physics in the model. In order to achieve a good agreement in DIII-D, the α-stabilisation had to be included into the model, emphasising the role played by the α-stabilisation in the physics of the ITBs. The Weiland and GLF23 transport models show limited agreement between the model predictions and experimental time evolution of the ITB and kinetic plasma profiles. TheWeiland model does not to form a clear ITB in any of the three tokamaks despite varying plasma profiles, such as the q-profile. On the other hand, the average temperatures and density are often in fair agreement with experimental values. The GLF23 model often predicts an ITB, but its radial location is often too far inside the plasma, or shrinks as the simulations proceed in time. Consequently, the central temperatures at the end of the simulations during the high performance phase are usually underestimated. Worth noting is that GLF23 features in general better predictions of the Te and Ti profiles outside the ITB than the other models studied. Achieving the quantitative capability to predict the multichannel ITB dynamics with fully predictive, time-dependent transport simulations has turned out to be extremely challenging.

1. INTRODUCTION

The accuracy of predictive transport modelling in plasmas with Internal Transport Barriers (ITBs) is not as good as that in the standard ELMy H-mode scenario. That is particularly evident in timedependent simulations where the discharge evolves from the early preheating phase towards the onset of the ITB while the q-profile is changing all the time. In addition, the other plasma profiles (density, ion and electron temperature and rotation) can change dramatically when turbulence becomes suppressed and/or heating power and momentum injection is increased. The difficulties in the time-dependent ITB simulations stems mainly from the following two facts: firstly, the ITB formation mechanisms are not yet fully understood [1, 2, 3] and secondly, time-dependent simulations are extremely challenging as the plasma profiles and transport processes are so interlinked with each other. Small, time-dependent variations in some plasma parameter or profile can cause the simulations easily to depart far from their present state. In addition, small differences in some plasma profile may move the discharge or the simulation over the threshold of the micro-instability, causing thus large differences in the predictions with time due to large changes, for example in the growth rates γ of some micro-instability (c.f. ITB appearance/disappearance).

Furthermore, predicting the whole process of the ITB formation and the simultaneous dramatic

changes in the plasma profiles challenge the transport models to be accurate under largely varying plasma conditions within one simulation. Due to the aforementioned problems, simplified and not self-consistent approaches, such as time-independent steady-state simulations or predicting only for example the ion and electron temperature profiles with the given experimental density, toroidal rotation and q-profile, are usually employed in predictive modelling of ITBs [4, 5, 6, 7]. On the other hand, these simplified timeindependent simulations are very useful in trying to explain for example the physics mechanisms governing the physics of the ITBs, to test the accuracy of different transport models in steady-state conditions, to predict whether we will obtain an ITB in ITER with given kinetic and q-profiles etc. The third lack in concluding on the results and capabilities of the transport models and simulations of ITBs is that there are only very few attempts to predict ITBs in the multi-tokamak ITPA (International Tokamak Physics Activity) ITB database [8]. As a consequence, the aim in this work is to consider and assess all the aforementioned three deficiencies in the present transport simulations — by making (1) fully predictive and self-consistent transport simulations carried out in a (2) time-dependent manner, and (3) comparing several transport models for discharges from three different tokamaks.

The leading candidates for ITB triggering and also governing the physics of the ITBs are the turbulence suppression by the !E B shearing rate [9, 10, 11, 12, 13, 14, 15, 16], by negative or small magnetic shear [17, 18, 19, 14, 20, 21, 16], by -stabilisation [19, 22, 23, 24], by a large density gradient [25, 26] and by the rational values of the q-profile [27, 28]. In this work, we have used three different transport models, the mixed Bohm/GyroBohm [14, 29], the Weiland [30, 31] and the 'retuned' GLF23 [11, 32, 4], to carry out all the transport simulations. However, none of these transport models includes all the enumerated ITB triggering and physics mechanisms, in particular none of the models addresses the effect of rational values of the q-profile. On the other hand, different transport models emphasise different ITB formation mechanisms more strongly and ignore some of them. Therefore, a success or a failure by some model under certain plasma conditions (for example reversed versus flat q-profile) or in some tokamak provides important information on the relative importance of $\omega_{E\times B}$ flow shear, magnetic shear, α-stabilisation, etc. in ITB formation. It may also reveal some ideas on what quantities to vary in order to control ITBs in an optimum way. This paper is structured in the following way. The simulation methodology adopted in this study and the used input data are illustrated in section 2. The transport codes jetto and cronos are described in section 3. In addition, a brief description of the transport models (Bohm/GyroBohm, Weiland and GLF23), including the possible turbulence stabilisation mechanisms in each model, is given. In section 4, the simulation results from the six modelled discharges are compared with the experiments. Section 5 is devoted to testing the sensitivities and robustness of fully predictive simulation results with respect to different versions of the models and layered tests. In addition, a statistical analysis of the simulation predictions is carried out to see prediction accuracy among the different tokamaks and transport channels. Finally, the conclusions with a summary are discussed in section 6.

2. SIMULATION METHODOLOGY AND SELECTION OF THE INPUT DATA

The selection of the simulated discharges was strongly inspired and encouraged by the International Tokamak Physics Activity (ITPA) group on transport and ITB physics and the earlier work carried out by the group [6]. In order to investigate to what extent the three transport models are capable of reproducing the time dynamics of the ITB pulses in the ITPA ITB database, three pairs of high performance discharges from JET, JT-60U and DIII-D are selected. Having discharges from three different tokamaks enables us to recognise common and non-common features of ITB formation and dynamics between different tokamaks. More importantly, it is possible to perform a fully predictive, time-dependent cross-tokamak ITB/transport model test—a critical step necessary to improve the predictive capability for the ITB plasma scenarios in the next step devices such as ITER. One of the discharges in each pair (each tokamak) has a flat q-profile whereas the other one has a strongly reversed q-profile in the high performance phase. This allows the self-consistent q-profile and magnetic shear evolution and dependencies predicted by the transport models to be compared with each other and with experiments on different tokamaks. The main plasma parameters for the six simulated discharges are presented in Table 1. The micro-stability analysis of the same discharges is performed in [23].

One of the fundamental principles in this work is to make fully predictive transport simulations. The concept of 'full predictability' means that five transport equations, i.e. ion and electron heat transport, main ion particle transport, toroidal momentum and current diffusion equations, are solved. Thus, the simulations yield predictions for T_i, T_e, n_i, v_ϕ and q, respectively. Predicting the density is important because the self-consistent interaction of the temperature and density and their gradients is crucial in the calculation of the growth rates of ITG and TEM. In addition, ITB formation is strongly affected by the density gradient [26]. Moreover, the off-diagonal contributions in the transport matrix, i.e. the density and temperature gradients, may cause heat and particle pinches, respectively, and thus influence the ITB dynamics significantly. In order to improve the reliability of the transport/ITB model and its predictive capability, it is of a paramount importance to solve also the toroidal momentum equation rather than use the experimentally measured value for v_ϕ. This is due to the key role played by v_ϕ in the value of the $\omega_{E\times B}$ flow shear (at least with unidirectional NBI). Using the experimental value of v_ϕ would give too strong indications to the ITB model where and when to form the barrier via imposing the increase in the $\omega_{E\times B}$ flow shear through the experimental v . In addition, this approach would break the 'full predictability' and self-consistency principles adopted in this work. Furthermore, extrapolation of the simulation predictions for the advanced tokamak scenarios to next step devices would be less reliable. However, at this point we need to note that the GLF23 transport model is for the present integrated only for energy transport in the cronos transport code [34], and thus, the experimental density and toroidal rotation are used for the simulations carried out with this model.

All the necessary input data for the three pairs of discharges from JET, JT-60U and DIII-D are taken from the international multi-tokamak ITB database [8]. The input data includes the geometry,

the power deposition profiles, the external non-inductive current sources, torque, Z_{eff} as well as the initial and boundary conditions for the transport equations to be solved. Although exactly the same experimental parameters and profiles exist in ITPA database from all the tokamaks, the way how the data is saved into the database is not uniform among the different tokamaks; JET discharges include a long preheating phase without an ITB whereas the DIII-D and JT-60U data focus on a time period corresponding to the ITB formation. Neo-classical quantities are calculated using the NCLASS transport code [35]. The simulations using the Bohm/GyroBohm andWeiland models are performed with the jetto transport code [36] and the simulations using GLF23 with the cronos transport code [34].

One of the main problems in time-dependent transport simulations, in particular in the multitokamak database and with several transport models, is that the input data and simulation procedures can be treated in various ways. As a consequence, in order to minimise their impact on the modelling results, we keep the simulation parameters and procedures as identical as possible — both among the simulations in different tokamaks and with different transport models. Although time steps and equilibrium are not done exactly in the same way in jetto and cronos, such differences do not induce any significant bias in the kind of comparisons carried out in this study. jetto and cronos transport codes were checked to give very similar results with the same input data when using a simple transport model as shown in section 3. Finally, the simulation results are handled equally when analysing the accuracy of the predictions.

The sensitivity and robustness of the fully predictive transport simulation results are analysed testing different versions of the models and carrying out layered tests. In a layered test, the simulation imposes one or some of the profiles, like q, ν_ϕ and/or n_e from the experiment while the other transport channels are predicted. Comparisons of the simulation and experimental results between the transport channels and different tokamaks are evaluated in a statistical way. The main emphasis in the transport model evaluation is on the radial location and strength of the ITB throughout the time evolution of the ITB. In order to diagnose the role of the the $\omega_{E\times B}$ shearing rate, the growth rates of the Ion Temperature Gradient (ITG) modes and Trapped Electron Modes (TEMs) calculated by the Weiland transport model and GLF23 transport model as well as those calculated by the gyrokinetic flux tube code kinezero [33], all the profiles are compared with each other. A more extensive micro-stability analysis of the same discharges using the ITPA ITB database is performed by C. Bourdelle et al. [23].

3. TRANSPORT MODELS AND CODES

The original semi-empirical Bohm/GyroBohm transport model in jetto [29] was amended to include the empirical ITB formation condition in Ref. [14]. The empirical ITB formation threshold condition was derived from the experimental JET database with discharges having ITBs with a low positive magnetic shear. Recently, this ITB formation condition was supported in Ref. [37] where also ITB discharges with a negative magnetic shear were used. The set of diffusion coefficients can be written

as follows:

$$\chi_e = 1.0\chi_{gB} + 2.0\chi_B + \chi_{neo-al} \tag{1}$$

$$\chi_i = 0.5\chi_{gB} + 4.0\chi_B + \chi_i^{neo} \tag{2}$$

$$D = (0.3 + 0.7\rho)\,\frac{\chi_e \chi_i}{\chi_e + \chi_i} \tag{3}$$

$$\text{where } \chi_{gB} = 0.5 \times 10^{-6} \sqrt{T_e}\,\left|\frac{\nabla T_e}{B_\phi^2}\right| \tag{4}$$

$$\chi_B = \chi_{B0} \times H\,(C_1 + s - C_3\,\omega_{E\times B}/\gamma_{ITG}) \tag{5}$$

$$\text{with} \quad \chi_{B0} = 0.5 \times 10^{-6}\,R\left|\frac{\nabla(n_e T_e)}{n_e B_\phi}\right|\, q^2 \times \left(\frac{T_e(0.8\rho_{max}) - T_e(0.8\rho_{max})}{T_e(\rho_{max})}\right) \tag{6}$$

$$\text{and } \chi_{neo\text{-}al} = \frac{c^2 v_{th}}{\omega_{pe}^2 qR} \in \square \tag{7}$$

In equations (4)–(7), T_e and T_i are the electron and ion temperatures, respectively, n_e is the electron density, B_ϕ the toroidal magnetic field, R the major radius, q the safety factor, c the speed of light and v_{th} and ω_{pe} are the electron thermal velocity and plasma frequency as well as R is the major radius and the inverse aspect ratio. All the neo-classical transport quantities, such as the neo-classical ion heat conductivity χ_i^{neo}, electrical resistivity, bootstrap current, etc., are calculated with nclass code [35], which is coupled to jetto and cronos. χ_{neo-al} term represents transport arising from the Electron Temperature Gradient (ETG) modes and has a similar form to one proposed by Ohkawa [38]. The non-locality in the Bohm transport appears in the last term where is the flux surface label defined by $\rho = \sqrt{\Phi/\pi B_\phi}$. ρ_{max} is the value of ρ at the separatrix in the L-mode and on top of the edge barrier in the H-mode and Φ is the toroidal magnetic flux. All the quantities appearing in Eqs. (1)–(7) are expressed in SI units except the temperatures T_e and T_i whose unit is eV.

ITBs are introduced with the Heaviside step function multiplying the modified Bohm transport in Eq. (5). The controlling parameter is given by the ITB formation threshold condition found in Ref. [14]. We fixed the empirical constants $C_1 = 0.1$ and $C_3 = 1.0$ because the optimum value for C1 varies between around 0 and 0.2 and for C_3 between 0.5 and 1.6 among the simulated discharges from each three tokamaks. Inside the argument of the step function, $\omega_{E\times B}$ is the flow shearing rate by Hahm-Burrell [12] and ITG is a simple approximation of the linear growth rate defined as $\gamma_{ITG} = v_{th,i}/R$ with $v_{th,i}$ being the ion thermal velocity. The $\omega_{E\times B}$ shearing rate is consistently calculated with the evolving plasma profiles at each time step in all the transport models. Mathematically, when the argument in the step function $C_1 + s - C_3\,\omega_{E\times B}/\gamma_{ITG} = 0$ changes its sign, the ITB either forms ($H(x < 0) = 0$) or collapses ($H(x > 0) = 1$). Physically, when the Bohm-type of anomalous transport χ_B is fully suppressed in Eqs. (1)–(3), the internal transport barrier forms.

The toroidal velocity is calculated from the momentum balance equation similarly to the other transport equations using the torque from the neutral beam injection as the source term. The anomalous toroidal viscosity coefficient is assumed to be equal to the ion heat transport coefficient as in Eq. (2). There is experimental evidence on JET and other tokamaks that in the NB heated plasmas, the toroidal viscosity coefficient coincides with the ion heat diffusion coefficient, both radially (at least inside r/a = 0.8) and with time [39]. The poloidal rotation is assumed to be neo-classical and is calculated by nclass.

In order to study the possible role of α-stabilisation with the Bohm/GyroBohm model, the ITB formation threshold condition, given in equation (5), was modified. At least for trapped electron modes, according to Ref. [40], stabilisation of the growth of the modes is predicted when the condition $3/8 + s - 3/5\alpha < 0$ is fulfilled. This equation is exact for trapped electrons in s–α equilibrium. For the ions the exact values for the coefficients 3/8 and –3/5 in the threshold condition depend on the poloidal mode structure. In the following approach, we will apply the same stabilisation criterion also to ions. When combining this expression with equation (5), the amended ITB threshold condition takes the following form:

$$\chi_B = \chi_{B0} \times \Theta\,(C_1 + s - C_3\,\omega_{E\times B}/\gamma_{ITG} - 3/5\alpha) \tag{8}$$

where is defined as normally in MHD, i.e. $\alpha = 2Rq^2\,\mu_0/B^2 dp/dr$ with p being the pressure and μ_0 the permeability of the vacuum. The numerical constant C_3 was kept in the same value (C_3=1.0) as in equation (5). In order to be as consistent as possible with the old (equation (5)) and new ($3/8 + s - 3/5\alpha < 0$) ITB threshold conditions, the numerical constant C_1 takes the value of 0.5. This stems roughly from the sum of the original $C_1 = 0.1$ (equation (5))and the new α-stabilisation term that requires $C_1 = 3/8$. Effectively, the new ITB threshold condition replaces the constant $C_1 = 0.1$ with $0.5 - 3/5\alpha$.

The transport coefficients in jetto with the implementedWeiland model can be described the following simplified way:

$$\chi_e = \chi_{e,weil} + 0.1\chi_B \tag{9}$$

$$\chi_i = \chi_{i,weil} + 0.1\chi_B + 0.1\chi_i^{neo} \tag{10}$$

$$D = D_{weil} + 0.1\chi_B \tag{11}$$

where $\chi_{e;weil}$, $\chi_{i;weil}$ and D_{weil} describe the effective transport coefficients from the ITG and TEM modes calculated by the Weiland model [30, 31, 41, 42, 43]. The standard version of the Weiland model [30] is used in all the transport simulations unless otherwise stated. It includes also the offdiagonal terms in the transport matrix (not explicitly shown in the equations (9) – (11)). The model includes the

following, also experimentally observed, micro-turbulence stabilisation mechanisms: Hahm-Burrell $\omega_{E\times B}$ shearing rate versus the instability growth rate, negative or small magnetic shear, α-stabilisation, dilution effects such as impurity content (Z_{eff}) and density gradient length versus the temperature gradient length. The $\omega_{E\times B}$ flow shear is calculated consistently with the varying plasma profiles inside jetto. The ITB formation can be caused by any of these alone or be a combined effect of some them. The standard version does not include the collisions and electro-magnetic effects. However, they are included in some of the simulations to assess their effect on the dynamics of the ITB evolution. In addition, a comparison between the standard version and the new version that includes a variable correlation length [46] is carried out. The new version takes the fastest growing mode from the perpendicular wave number spectrum instead of the fixed one which corresponds to the inverse correlation length in the standard model. This new version has a stronger dependence, for example on magnetic shear and plasma geometry, such as elongation. Therefore, it may result in different predictions for ITBs in plasmas with negative or small magnetic shear.

The reason for using additional 10% of the Bohm transport in equations (9) – (11) is to improve the numerical stability of the simulations. It mainly increases edge transport outside the core region $\rho > 0{:}8$ as the Bohm tends to increase strongly towards the edge due to q^2 dependence. In many cases without the extra 10% of the Bohm term, these long, time-dependent simulations either crash or suffer from severe numerical instabilities. On the other hand, 10% of Bohm transport is negligibly small compared with $\chi_{i;weil}$ and $\chi_{e;weil}$ in the core region. Comparing two identical simulations, but one with and one without the extra Bohm term, gives very marginal difference in the overall temperature and density profiles even after 3s of simulation time in a non-steady state plasma, but as a benefit one obtains numerically much more stable simulations. This is illustrated in figure 1. As can be seen, a numerical instability is growing at $\rho = 0.1$ in the simulation without the additional Bohm transport. As a very important detail, there are no empirical or numerical fitting parameters in the present jetto implementation of the Weiland model.

The simulations using the GLF23 transport model [11, 32, 4] have been performed with the cronos transport code, in which the v1.61 'retuned' version of GLF23 has been implemented. The electron and ion temperatures and the q-profile are predicted while densities and toroidal rotation are fixed to their experimental values. The ion densities (deuterium and carbon) are calculated from the experimental electron density and Z_{eff} profiles, read from the ITPA ITB database. Since the GLF23 model does not usually give satisfactory agreement in the outer part of the plasma (at the plasma edge) $\rho > 0{:}8$, the mixed Bohm/GyroBohm model is used for the prediction in this outer region. Also, the ion neoclassical diffusivity is used as a lower bound for the thermal diffusion coefficients, both in ion and electron channel. This prevents numerical instabilities where the GLF23 model predicts an anomalous transport equal to zero. The model includes qualitatively the same micro-turbulence stabilisation mechanisms as the Weiland model, i.e. $\omega_{E\times B}$ shearing rate, negative or small magnetic shear, α-stabilisation, the dilution effects and density gradient length versus the temperature gradient length. However, the heat fluxes are calculated in GLF23 using a very different

approach with respect to the Weiland model, since its linear growth rates and frequencies are fitted to the results of full linear gyrokinetic calculations [4]. In addition, in GLF23 the $\omega_{E\times B}$ shearing rate is calculated by the Waltz formula [11] inside the GLF23 module, consistently with the profiles provided by cronos, rather than employing the Hahm-Burrell formula [12] as employed by the Bohm/gyroBohm andWeiland models. Worth noting is that none of the three transport models takes into account any possible role played by the rational surfaces of the q-profile.

Since the GLF23 model is quite sensitive from the numerics point of view, it requires in some cases the use of very low time steps (of the order of 10^{-6}s) in the transport equation solver. This is a strong constraint for simulations of several seconds of plasma discharges, therefore the usual strategy adopted in cronos is to smooth radially the GLF23 output diffusion coefficients (3 neighbouring grid points averaging method, using a radial grid of 101 points). This mild smoothing procedure allows to run fast and reliable simulations with time steps of the order of $10^{-5} - 10^{-4}$s. It does not prevent the formation of strong temperature gradients comparable to those usually found in ITB discharges. It has been checked that this procedure yields the same temperature profile predictions as the simulation without smoothing using a much smaller time step, on a test case featuring an ion ITB of characteristic scale length $T_i/(dT_i/dr) \approx 0.08$m. This scale length is typical of the ion ITBs studied in this work.

JETTO [36] and cronos [34] are both one and a half dimensional integrated transport modelling codes solving the time-dependent transport equations averaged over the magnetic flux surfaces. There are several options for example for the equilibrium calculation, handling the heating and current drive, boundary conditions etc. in the codes. We have always used as consistently as possible the same code options, described in more detail below, in all the jetto and cronos simulations performed during this study.

In order to be most consistent between the simulations, the input data from the ITPA ITB database has been used as thoroughly as possible. This makes the comparisons of the simulation predictions between the discharges and tokamaks most 'code and modeller' independent. As a consequence, the external power deposition and driven current density profiles by NBI and ICRH as well as torque and Z_{eff} are taken from the ITB database. In addition, the initial conditions for n_e, T_e, T_i, q and v_ϕ as well as the boundary conditions for the same quantities are taken from the database. The boundary conditions are enforced on top of the H-mode pedestal, and this location corresponds to the $\rho = 1.0$ surface where ρ is the normalised toroidal flux coordinate. The boundary conditions for the current diffusion equation, i.e. the q-profile evolution, is the total plasma current, taken from the database.

The equilibrium is solved with the esco [36] equilibrium solver that is inside jetto and with helena [44] in cronos. The equilibrium is recalculated self-consistently with the varying pressure and current density profiles during all the simulations. All the necessary quantities (toroidal magnetic field, major and minor radii, ellipticity and average triangularity of the last closed flux surface) for the equilibrium reconstruction are read from the ITB database.

In order to ensure that the use of three transport models in two different transport codes, Bohm/ gyroBohm and Weiland models in JETTO and GLF23 in CRONOS, does not yield any bias to the simulation results, two benchmark cases between the two codes were carried out. In the first one, the ion and electron thermal diffusion coefficients calculated with cronos are given as input in JETTO to compare the predicted temperature profiles. The comparison is shown in figure 2(a). The predicted temperatures with the two codes are almost identical, indicating that the different equilibrium, grid sizes and numerical algorithms do not lead to any undesirable bias in the predictions between the two codes. The second benchmark case was performed with the 'retuned' GLF23 transport model, both with cronos and jetto. The simulations were run in a reduced way, i.e. switching off the !E B flow shear and α-stabilisation and excluding fast ions. In addition, exactly the same input file with density, q-profile and power deposition profiles was used. Besides the diffusion coefficients from GLF23, the neo-classical transport, calculated separately in each code with nclass is added. The benchmark simulations are shown in figure 2(b). As can be seen, both jetto and cronos codes predict very similar ion and electron temperatures as well as ion and electron thermal diffusion coefficients.

In addition to benchmarking GLF23 between cronos and jetto, the GLF23 model in cronos has also been extensively benchmarked against the GLF23 model in xptor transport code [45]. For an L mode discharge, a good agreement is found between the two codes, i.e. the predicted temperatures agree within a deviation of 7%. This deviation is not ascribed to a different implementation of the GLF23 in the two codes, but to unavoidable differences in the integrated calculation between CRONOS and XPTOR (for example electron-ion heat transfer and ohmic heating could not be matched exactly for technical reasons). This benchmark exercise has been also carried out on a single time slice simulation (calculation of the stationary solution) for DIII-D shot no. 95989, t = 0.88s, which features an ITB. The xptor result for this simulation has been published in [4] (Fig.10 in that reference), showing an excellent agreement with the experimental data in reproducing the ion ITB, while not predicting the electron ITB as, however, observed experimentally. The same simulation has been done with cronos, using the same version of the GLF23 model and input data from the ITPA ITB database as described above. The cronos results are qualitatively similar to those of xptor; a similar ion ITB is predicted while no electron ITB is predicted. The ion ITB found by cronos has the same ion temperature gradient inside the ITB, but is slightly narrower (ITB foot at $\rho = 0.3$ instead of $\rho = 0.4$, resulting in lower central ion temperature (8 keV instead of 12 keV). This discrepancy maybe be ascribed to differences in input data and numerical schemes. Indeed, reference [4] has used directly data from the DIII-D database which may differ from that submitted to the ITPA ITB database. Unfortunately, it has not been possible, for this test case, to retrieve the input data that has been used in ref. [4] in order to do a fully comparable simulation with cronos. As a consequence, it is not possible to quantify the deviation that could arise from the use of different numerical schemes in the comparison with ref. [4]. In any case, this benchmarking activity has shown the sensivity of the simulations results with the GLF23 transport model in ITB plasmas with

respect to variations, for example in number of grid points, q-profile, Z_{eff}, etc. And most importantly, this benchmarking exercise has allowed to check carefully the implementation of GLF23 and to certify that the input and output of the model were used properly within cronos.

4. COMPARISON BETWEEN THE SIMULATION RESULTS AND EXPERIMENTAL DATA

The time evolution of one of the simulated discharges with a monotonic q-profile (Pulse No. 46664 in JET) is illustrated in figure 3 (solid curve). The simulation predictions with the Bohm/GyroBohm (dashed), theWeiland (dash-dotted) and GLF23 (dotted) models are also shown. This discharge illustrates well the different phases of the plasma evolution, starting from the early preheating phase at t = 3s, advancing towards the main heating phase (t = 4.8s) and finally reaching the fully established ITB at t = 5.7s (disrupted after t = 6s). In the coming analysis of the plasma profiles, the instants of the plots have been chosen to be at the latest time available in the database, which corresponds to the fully developed ITBs. However, in the statistical analysis, all the profiles at each simulated time point from the start until the end of the simulations have been used when calculating the mean and standard deviation of the discrepancy between the predictions and experimental data.

Figures 4–6 illustrate all the simulated profiles for T_i, T_e, n_e, v_ϕ and q for the three pairs of discharges from JET, JT-60U and DIII-D in the respective order at the end of each simulation. In all the three figures, the label scheme is as follows: the solid curves correspond to the experimental data from the ITPA ITB database, and the dashed, dash-dotted and dotted curves to the simulation predictions by the mixed Bohm/GyroBohm, Weiland and GLF23 transport models, respectively. Also in each figure, the plots on the left-hand side present the data and simulation results for the discharge with a monotonic or flat q-profile and on the right-hand side for the discharge with a reversed q-profile in each tokamak, respectively.

The predictions with the Bohm/GyroBohm model show fair agreement with experiments for JET discharge no. 46664 (positive shear). Although the ion and electron temperatures are overestimated, the radial location of the ITB and toroidal rotation are almost perfectly matched. On the contrary, the Weiland model fails to trigger the ITB and thus underestimates the central ion temperature and toroidal rotation significantly. Both the Bohm/GyroBohm and Weiland models underestimate the heat transport outside the ITB ($\rho \leq 0.5$) while the density is well reproduced. On the other hand, GLF23 reproduces particularly well the anomalous heat transport outside the ITB, as shown in the temperature profiles. It predicts very well the existence of an ion ITB until t = 5.5s (see figure 3, T_i on top graph), but after that the ITB collapses, and the central T_i and T_e are strongly underestimated. The predicted q profile by all models matches well with the reconstructed one in figure 4.

For JET Puls No: 53521, the Bohm/GyroBohm model predicts the ITB 10cm too wide, and thus overestimates the ion temperature. No clear ITB in the electron temperature profile is predicted although the central value agrees well with the experimental one. The Weiland model underestimates

the heat transport outside the ITB which leads to the overestimation of T_i and T_e. The GLF23 model predicts a strong ITB at $\rho = 0.5$ instead of $\rho = 0.35$ that is observed in the experiment. The Bohm/gyroBohm and GLF23 models predict well the location of the minimum value of q at $\rho \approx 0{:}3$ although the value of q in the centre is underestimated.

The agreement between the experimental and simulated data with the Bohm/GyroBohm model is good in JT-60U, in particular with respect to the radial location of the ITB. Interestingly, with the positive shear, the model overestimates T_e and n_e whereas with the negative shear, it does quite the opposite while the ion temperature matches the experimental value well in both cases. The toroidal rotation is practically zero in JT-60U as the balanced NBI does not give any momentum source, i.e. torque is zero. In neither case does the Weiland model exhibit an ITB nor a good agreement with experiments. The GLF23 models gives rather accurate temperature predictions outside the ITB, but does not predict the ITB properly for those two shots. Only a very narrow ITB at $\rho = 0.2$ is obtained for Pulse No: 34487, while the foot of the ITB in the experiment is at $\rho = 0.6$. No ITB is predicted for Pulse No: 39056. Owing to the high q value in the core of Pulse No: 39056 (current hole), the neoclassical heat diffusion coefficients are very high ($10 m^2/s$ for the ion channel), providing flat temperature profiles inside $\rho = 0{:}4$.

JT-60U pulse no. 39056 has almost a current hole in the centre (q approaching infinity) as shown by the solid curve in figure 5(j). In transport codes, the maximum value of the q-profile must be limited in order to prevent the simulations from crashing. This limit, which is in this case $q_{max} = 30$, is one reason for the predicted q-profile to deviate from the reconstructed one. There are two reasons why the predicted q-profiles between the two transport models (dashed versus dash-dotted), and also between the experimental one (solid), look so different with each other. Firstly, the bootstrap current is very large (about 65% of the total current) with the prediction of the Bohm/GyroBohm model due to the strong ITB (pressure gradient) and much smaller (about 30% of the total current) with the prediction of theWeiland and GLF23 models with small pressure gradient. Secondly, the lower T_e predicted by theWeiland and GLF23 models enhances the current penetration to the centre of the plasma. In all the other five discharges (they do not exhibit a current hole), the agreement between the simulated and experimental q-profile is better, in particular with the Bohm/gyroBohm model. The agreement for the prediction of the q-profile depends on the prediction accuracy for the location and strength of the ITB, with the location and strength being directly linked to the location and amount of the driven bootstrap current, respectively.

In DIII-D, the Bohm/GyroBohm model does not predict the shape of T_i and n_e profiles as well as in JET and JT-60U. In addition, the radial location of the ITB is somewhat overestimated, typically by $\rho \approx 0.15$. Furthermore, the model has large difficulties in predicting correctly the shape of the toroidal rotation profile. The disagreements are firstly due to the fact that there is no ITB in the density profile in the experimental data whereas the simulations predict that and secondly, the ion temperature and toroidal rotation profiles peak towards the magnetic axis, not predicted by the model. By the construction of the Bohm/GyroBohm model, it can only predict ITBs for each transport

channel (T_i, T_e and n_e) at the same radius and simultaneously and thus, it cannot predict the aforementioned differences in the profiles between the different transport channels. The qualitative difference in the shape of the experimental plasma profiles (T_i and v_ϕ peaking and no ITB in n_e) between DIII-D and JET or JT-60U indicates that the ITB dynamics and turbulence may be governed by other mechanisms than those in JET and JT-60U. In order to obtain a better consistency in the accuracy of the predictions over the various tokamaks, the simulations with the -stabilisation (Shafranov shift) in the Bohm/GyroBohm model are carried out in section 5.

The Weiland model fails to reproduce an ITB and the shape of the plasma profiles in either DIII-D pulse. However, transport outside the location of the ITB is better reproduced in DIII-D than in JET or JT-60U. Reproducing the ion temperature and toroidal rotation seems to be again the biggest problems. The GLF23 model predicts for both DIII-D shots too narrow an ITB at $\rho = 0.3$, whereas in the experiments the ITB foot is around $\rho = 0.4 - 0.5$. Note that for the Pulse No: 95989, the model predicted an ITB in the ion channel only, whereas a clear ITB is also observed in the electron channel in the experiment, as shown in figure 6(d).

5. SENSITIVITY AND STATISTICAL ANALYSES OF THE SIMULATION PREDICTIONS

The effect of the α-stabilisation with the amended ITB threshold condition (equation (8)) is illustrated in figure 7 for the two DIII-D discharges. The experimental data (solid curves) and the predictions by the standard Bohm/GyroBohm model (dashed curves) are the same as in figure 6 whereas the dash-dotted lines correspond to the simulations with the amended model with the α-stabilisation. The agreement between the experiments and modelling improves in all respects (except maybe the marginal decrease in T_e) after the inclusion of the α-stabilisation term, for either DIII-D discharge, independently of the difference in the q-profile and magnetic shear. The radial location of the foot of the ITB has moved inwards with respect to the previous simulations, being in better agreement with the experiment for T_i and v_ϕ. Thus, since the ITB shrank radially (approximately by $\rho \approx 0.1$), it indicates that the new ITB threshold condition has larger values around the ITB location than the old one, i.e. $0.5 - 3/5\alpha > 0.1$. In addition, the modified model predicts somewhat stronger peaking towards the axis in Ti than the old one, similarly to that observed in the experiments. Still, the model does not predict the toroidal rotation profile well, in particular with the flat q-profile (pulse no. 87031). Moreover, since the Heaviside function for describing ITBs is applied to all transport channels in the model, an ITB is also predicted for ne while this does not appear in the experiment.

The same simulations, with the -stabilisation included according to equation (8), were also repeated for JET and JT-60U discharges. The simulation results between the old and new ITB models were very similar. Only in one case (JET Pulse No: 53521), the central ion or electron temperature changed more than 1 keV. In all the four cases, the footpoint of the ITB changed less than $\rho < 0.05$, being closer to the experimental footpoint of the ITB in two cases and further also in two cases than in the simulations without the α-term. The comparison of the new and old ITB

threshold conditions gives approximately $0.5 - 3/5 \approx 0.1$ in JET and JT-60U. This indicates that the value of is larger in JET and JT-60U than in DIII-D, at least around the ITB. In JET and JT-60U, the effect of α is hidden, possibly by coincidence, in the value of constant C_1 while in DIII-D, α must be taken as an explicit contributor to the ITB formation threshold condition, in particular to account for the ion ITBs in DIII-D.

It is quite solid to state that the standard Weiland model is not capable of predicting the time evolution of ITB plasmas satisfactorily in the multi-tokamak database, when the simulations are done in a fully predictive way. On the other hand, it has been successful in reproducing ITBs in some simplified steady-state simulations [46]. Even if the time traces of the volume averaged ion and electron temperatures and density are often in fair agreement with the experiments, the model does not predict a clear ITB for any of the simulated discharges, in spite of the varying plasma conditions with different discharges on different tokamaks. There are probably several, accumulated reasons for the failure. One of the most obvious reasons is illustrated in figure 8. The linear growth rates presented in figure 8 are shown before the subtraction of the $\omega_{E\times B}$ shearing rate. The linear growth rates calculated by the Weiland model exceed the $\omega_{E\times B}$ shearing rate by a factor of 2–10, depending on the discharge. In order to trigger an ITB, the $\omega_{E\times B}$ flow shear must be multiplied artificially typically by a factor of about 10 even if the ratio $\gamma/\omega_{E\times B}$ would be less than 10. This is because the artificially increased shearing rate decreases gradually transport which then allows the temperature profiles to become steeper, and this further leads to increased growth rates, and to compensate these, the $\omega_{E\times B}$ shearing rate needs to be further increased. This seemed to be true at least in JET and DIII-D where the dominant contribution to the $\omega_{E\times B}$ flow shear comes from the toroidal rotation due to unidirectional NBI.

However, although the $\omega_{E\times B}$ shearing rate is too small to suppress the growth of the microturbulence within the ITB, ultimately, the problem in predicting ITBs with theWeiland model seem to originate from large, oversize growth rates. Oversize growth rates in ITB plasmas, as compared with the $\omega_{E\times B}$ shearing rate, predicted by the Weiland model in ITB plasmas are recently reported in [47]. On the other hand, the growth rates and profiles predicted by the Weiland are typically in good agreement in standard ELMy H-mode plasmas [48]. Therefore, the oversize growth rates predicted by the model seem to peculiar only to ITB plasmas. As a comparison, the growth rates calculated with the kinezero gyro-kinetic code are illustrated in figure 8 by the dotted lines. The growth rates represent the maximum growth rate in the region $k_\theta\rho_i < 2$ with k_θ being the poloidal wave number of the mode and i the ion larmor radius. This region is characteristic for the ITG and TEM instabilities. The temperature and density profiles, q, Z_{eff} and all the needed plasma parameters are taken from the corresponding jetto simulations with the Weiland model at the same time as the plasma profiles shown in figures 4–6. As can be seen, the growth rates calculated by the Weiland model are systematically larger than those calculated by kinezero for all six discharges. Although the comparison of the growth rates and shearing rates is rather naive, it actually reveals again the generic issue of the fluid models, like theWeiland model, as compared with the kinetic

models – the thresholds of the instabilities are significantly lower in fluid models than in kinetic models [49]. A more extensive micro-instability study of the same discharges with kinezero using the experimental plasma profiles from the ITPA database is reported in [23].

In order to test whether the different versions of the Weiland model result in improved agreement with the experimental data, simulations with two other versions of the model are compared. In the first one, the Electro-Magnetic (EM) effects and the collisions (dotted curves) are switched on (in the standard version of theWeiland model used so far they were switched off). Furthermore, simulations with the newest published version of the model [46], including the variable correlation length (dash-dotted curves) as described in section 3, are compared to the ones with the standard model (dashed curves) and experiments (solid curves). This comparison is illustrated in figure 9. Neither including collisions and EM effects nor including the variable correlation length improves the prediction accuracy significantly with respect to dynamics of the ITBs and in fact, the overall changes in the plasma profiles are very minor. The differences in the simulation results between the three versions of the model are also very small for the other discharges studied in this work.

In order to test the sensitivity and robustness of the fully predictive modelling results, layered simulations with one or several transport channels fixed to their experimental values or otherwise fixed plasma profiles are performed. One sensitivity test with the Weiland model is illustrated in figure 10 where two new simulations are compared with the experimental profiles (solid curves) and the fully predictive simulation (dashed curves) for JET Pulse No: 46664 at t = 6.0s. The first one (dotted curves) employs experimental density, toroidal rotation and q-profile throughout the whole simulation in time, thus yielding predictions only for T_i and T_e. The second one (dash-dotted curves) takes the toroidal rotation from the experiment, and uses a fixed, artificially strongly reversed q-profile, yielding predictions for T_i, T_e and n_e. The predictions both for the ion and electron temperatures remain almost unchanged when the experimental density, toroidal rotation and q-profile is imposed. Furthermore, even when using fixed, strongly reversed q-profile throughout the 3 second's simulation interval does not change the predictions for the temperatures or density significantly. Other layered simulations, for example with fixed temperature profiles, but with predicted n_e and v_ϕ etc. yielded consistently very similar results to the fully predictive simulation, in particular with respect to the existence of the ITB. Consequently, it is easy to conclude that the simulation predictions performed in a fully predictive mode are very robust and not very sensitive to changes in the q-profile, density or toroidal rotation. On the other hand, as the model does not predict ITBs, the present version of the model cannot be regarded as a satisfactory tool in investigating or developing advanced tokamak scenarios with ITBs, for example in view of ITER.

The GLF23 model predicts the ITB (in five of the six simulated discharges), unlike theWeiland model, but the footpoint of the ITB is located too far inside the plasma. As a result, the prediction for the central temperatures is underestimated. This conclusion is quite different from the results obtained by Kinsey et al. in Ref. [4] where a much better agreement is found on the ITB prediction using GLF23 for the two DIII-D discharges. One of these is even the same with the present work (DIII-D

95989, at t = 0.88s), and GLF23 provides in that reference a correct prediction of the ion ITB, slightly broader than our present results. A first difference between the two modelling studies is that we carry out time-dependent simulations of the discharges over several energy confinement times, while in ref. [4] GLF23 is used to find a stationary solution at a given time slice. However, this difference is not the main source of discrepancy between the two modelling results in the case of Pulse No: 95989. Indeed, we have also run a stationary simulation of time slice t = 0.88s, and found only small differences with the dynamical simulation (in the latter, the central temperatures are about 600eV lower). As discussed previously, the most likely cause of the difference between our present result and the one presented in ref. [4] is the distinct input data. Indeed, input parameters like electron-ion heat transfer, ohmic heating power, the toroidal velocity profile, etc. are different and consequently have a significant influence on the location of the ITB. This further emphasises the sensitivity of the ITB prediction to the various input parameters and thus the difficulty to obtain a reliable integrated simulation of ITBs in general.

The growth rates predicted by the GLF23 transport model are compared with the $\omega_{E\times B}$ rates in figure 11. The $\omega_{E\times B}$ shearing rate is calculated internally inside GLF23, and features a lot of spikes when a large number of radial grid points are used (101 points here. The numerical scheme used inside GLF23 for the evaluation of the second order radial derivative of the ion pressure, which is involved in the $\omega_{E\times B}$ shearing rate, seems not well adapted for such a detailed radial grid. However, the profile of the maximum growth rate is much smoother. ITBs are predicted by the model when !E B exceeds the local maximum growth rate (at = 0:5 for JET 53521, and around $\rho = 0.2 - 0.3$ for the DIII-D shots, JT-60U pulse no. 34487, and JET pulse no. 46664). In the case of JT-60U current hole shot, as explained above, the neoclassical coefficients are very high and provide flat temperature profiles, so that the growth rates from GLF23 are equal to zero inside ρ = 0:4. For the DIII-D and JT60U discharges, the $\omega_{E\times B}$ shearing rate is quite close to the maximum growth rate around $\rho = 0.5$ 0.6, i.e. where the ITB occurs in the experiment. Therefore, the model is close to triggering wider ITBs which would be at the correct radial location. The observed disagreement between the model predictions and the experiment (too narrow ITB or no ITB at all) might be solved by a small adjustment of the turbulence stabilisation mechanisms in the model. On the other hand, this result shows that the ITB prediction is quite sensitive, which explains why it is so challenging to model the dynamics of ITBs in time-dependent simulations. Finally, it should be noted that GLF23 features in general better predictions of the T_e and T_i profiles outside the ITB than the other models used here. Indeed GLF23 provides an accurate prediction of the temperature profiles outside the ITB for 4 of the 6 shots studied.

The statistical analysis of the simulation results was carried out by calculating the mean errors and standard deviations from the hundreds of evenly in time distributed plasma profiles, saved during each time-dependent simulation. In the case of ITB formation and non-stationary plasmas during the simulation, as in this study, this is probably the most sensible way to compare the simulation results in a statistical manner although the interpretation of the modelling offsets and standard deviations is not straightforward.

According to the statistical analysis, the standard deviations are clearly smaller in JET and JT-

60U than those in DIII-D, in particular with the Bohm/GyroBohm model. This can be interpreted that the main mechanisms in the transport model (s, $\omega_{E\times B}$ and α-stabilisation) that govern the dynamics of the ITB might be different or playing different roles in DIII-D from those in JET and JT-60U. After including the α-stabilisation in the model, the difference in the modelling accuracy between DIII-D and JET or JT-60U decreased, in particular in the ion heat and toroidal velocity transport channels. One reason for the dissimilar accuracy for the predicted plasma profiles by the model could be the size of DIII-D that differs from that in JET and JT-60U. This demonstrates the common problem when using semi-empirical transport models – the uncertainties in the scaling with the size may be significant.

Another conclusion is that the agreement between the simulations with the Bohm/GyroBohm model and experiments is better in plasmas with a flat q-profile than with a reversed one. This may be an indication that the turbulence suppression by the negative magnetic shear is different than predicted by the model in equation (5).

By comparing the predictions with the Bohm/GyroBohm model between the different transport channels one can conclude that the electron heat channel is best reproduced. The ion heat and particle transport channels still fall typically within the category of acceptable prediction accuracy whereas the toroidal rotation is beyond the reasonable accuracy. In the case of the Weiland model, the agreement between the experiments and simulations is poorest in the ion heat and toroidal rotation transport channels. This is probably because of more clear ITBs appearing in those two channels due to the dominant ion heating. In the case of poor predictions for v_ϕ, the approximation that the anomalous toroidal momentum diffusivity (viscosity) equals to the ion heat diffusivity does not seem to be a valid one. According to the statistical analysis, in order to best improve the predictive capability of both the Bohm/GyroBohm and Weiland transport models in ITB plasmas, understanding of the momentum transport, i.e. the role of anomalous viscosity must be increased. What is remarkable with the GLF23 model is that it the only model providing more accurate predictions for the ion temperature profiles than for the electron temperature profiles.

6. SUMMARY AND CONCLUSIONS

The predictive capabilities of three transport models, Bohm/GyroBohm,Weiland and GLF23, have been investigated with fully predictive, time-dependent simulations in ITB plasmas, taken from the ITPA ITB database. The main emphasis was on the prediction accuracy of the time evolution for the radial location and strength of the ITB. The experimental data from the ITPA ITB database provided the basis for performing the multi-tokamak transport model comparisons. Two discharges from JET, JT-60U and DIII-D were simulated with jetto and cronos transport codes.

The Bohm/GyroBohm model predicted the evolution for the location and strength of the ITB as well as the profiles of T_i, T_e and n_e within a fair accuracy in JET. This fair predictive capability of the Bohm/GyroBohm model in JET was somewhat expected because the ITB threshold condition was derived using the ITB discharges from JET [14]. On the other hand, it was derived using only

ITB discharges with zero or positive magnetic shear and therefore, it could have been not applicable to JET plasmas with a negative shear. As pulses from three tokamaks and with varying q-profiles have been simulated, this study has been a thorough test of the model.

What was astonishing to some extent was that the predictions with respect to the evolution of the strength and location of the ITB with the Bohm/GyroBohm model using the same ITB formation condition were in better agreement with the experiments in JT-60U than in JET. In addition, the balanced NBI in JT-60U creates almost no toroidal rotation, causing the !E B shearing rate to be born almost purely from the pressure gradient and poloidal rotation. This is in contrast with JET and also DIII-D where the main contributor to the $\omega_{E\times B}$ shearing rate is the toroidal rotation.

The agreement of the predictions by the Bohm/GyroBohm model was poorer in DIII-D as in JET or JT-60U. The radial location of the ITB at the end of the simulation was overestimated approximately by $\rho \approx 0.10–0.15$ and the model did not predict the peaking of T_i and v_ϕ towards the axis. Therefore, the ITB formation threshold condition was modified to include the effect of the α-stabilisation, as shown in equation (8). This modified ITB threshold condition reproduced the location of the ITB and the shape of the plasma profiles better than the ITB condition without the -stabilisation in DIII-D. On the other hand in JET and JT-60U, the difference between the simulations with and without the α-stabilisation term was less than 10 %. In conclusion, the best agreement with the Bohm/GyroBohm transport model in the multi-tokamak ITB database is achieved when the α-stabilisation is taken explicitly into account, as shown in equation (8).

The Weiland model does not predict the time evolution of the ITB plasmas satisfactorily in the multi-tokamak database. It did not predict a clear ITB for any of the simulated discharges. Because of this, it tended to underestimate the central ion temperature although the volume averaged temperatures and density were in fair agreement with the experiments. One of the main reasons for the unsatisfactory performance of theWeiland model seemed to be the oversize growth rates of the unstable modes (ITG, TEM, ...) in these ITB plasmas, calculated by the model. It seems plausible that using the Waltz rule with the Weiland model with a constant multiplier is too simplified an approach when performing fully predictive, time-dependent transport simulations.

Besides the standard version of the model, two other versions of the model were tested. However, the version with collisions and electro-magnetic effects switched on yielded very similar simulation predictions to the ones with the standard model. In addition, the simulations with the version having the variable correlation lengths were very similar to ones with the standard version.

In addition to testing different versions of the model, layered tests with the standard version of the model were carried out to study the sensitivity and robustness of the simulation results with respect to variations in plasma profiles. Fixing the density, toroidal rotation and the q-profile to their experimental values did not change the predictions for the temperatures as compared to the predictions with the standard version, at any instant of the simulation between the preheating phase (low temperatures) and the high performance phase (high temperatures). Even the simulation with fixing and enforcing the q-profile artificially to a strongly reversed one, instead of the monotonic

one and using the experimental toroidal rotation did not result in significant changes in the predicted temperature profiles. As a consequence, the Weiland model seems to have only a weak dependence on the magnetic shear and q-profile. Based on all the results above, it can be concluded that the simulation results are very robust both with respect to different versions of the model and large variations in plasma profiles. On the other hand, as the model does not predict ITBs, the present versions of the model cannot be regarded as a satisfactory tool in investigating or developing advanced tokamak scenarios with ITBs, for example in view of ITER.

The GLF23 model predicted the existence of an ITB (in five of the six simulated discharges), but the footpoint of the ITB was located too far inside the plasma (except for JET Pulse No: 53521, where the predicted ITB was too wide). In some cases it predicted the ITB in the ion channel only, even though an ITB exists also in the electron channel in the experiment (DIII-D 95989). However, the !E B shearing rate is usually close to quenching the turbulence at the correct radial location with respect to the ITB in the experiment. This shows the sensitivity of the ITB prediction in this model. In spite of the GLF23 model having been shown to be rather accurate in single time slice stationary ITB simulations [4], our results show that its predictions are not robust enough in time-dependent simulations reproducing the ITB dynamics. However, GLF23 features in general better predictions for the T_e and T_i profiles outside the ITB than the other models used here.

There are other references both with the Weiland model [46] and GLF23 [4, 45] stating that ITBs can be reproduced satisfactorily in many plasmas (Ref. [45] did not use the 'retuned' version of GLF23). However, there are three significant differences between those and the present simulations. Firstly, the simulations cited above have been run to find a stationary solution at a given time slice while the present simulations predict the whole time evolution of the discharge, including often the preheating phase. Secondly, the input data is distinct at some parts among the simulations between the different references, as the local databases usually differ to some extent from that of the ITPA ITB database. And thirdly, the present simulations have been fully predictive with the Bohm/gyroBohm and Weiland models whereas the simulation in Ref. [46] imposes experimental density, toroidal rotation and q-profile. The simplified time-independent simulations [46, 4, 45] are indeed very useful for example in studying the physics mechanisms governing the physics of the ITBs, to test the accuracy of different transport models in steady-state conditions, to predict whether we will obtain an ITB in ITER for example with given density and q-profiles etc. On the other hand, when the aim is to investigate and develop advanced tokamak scenarios as a whole issue, fully predictive, time-dependent transport simulations are needed. However, there is still a long way to go in order to understand the self-consistent evolution between the electron and ion temperatures, density, toroidal rotation and q-profile in transport simulations with ITBs.

None of the transport models assesses the role of the rational surfaces of the q-profile as a mechanism to trigger the ITB. This might be one of the reasons why the models are not very successful in reproducing the time dynamics of the ITBs. There is strong evidence on JET [27], but also on JT-60U [52], DIII-D [53] and RTP [54] that the rational surfaces play a significant role, at

least in triggering ITBs. The island structure on a rational surface can locally increase the $\omega_{E\times B}$ shearing rate which can lead to the ITB formation and then further increase of the $\omega_{E\times B}$ shearing rate. After having triggered the ITB, the role of the rational surface of q may vanish while the 'usual' turbulence stabilisation mechanisms take over. As a consequence, triggering ITBs might be dominated by a different process than dynamical time evolution, expansion and collapse of the ITB. The present transport models do not take into account possible triggering processes as a separate event from the ITB formation/dynamics. In order to resolve and model this issue, relevant MHD equations [55] should be coupled with the transport codes.

It is not maybe astonishing that it is extremely challenging to predict the evolution of the ITBs very well with fully predictive, time-dependent transport simulations. This is due to the fact that even experimentally, there are many open questions related to the physics of the ITBs. There are open questions about triggering mechanisms, bifurcative or continuous process, power thresholds, dominating turbulence suppression mechanisms, ITBs on different transport channels, weak versus strong ITBs etc. As already discussed above, there are no separate ITB triggering mechanisms in transport models, besides the normal turbulence suppression mechanisms discussed in section 3. Another open question is the existence of a power threshold and the nature of the onset of the ITB, bifurcative or continuous. The new evidence from JET seems to indicate that the transition from a non-ITB state to an ITB one is not necessarily a bifurcation, but rather a continuous process with no obvious power threshold [50]. In addition, the minimum power level required to observe a local

transport reduction is significantly lower than the value at which very steep pressure gradients can be achieved [51]. Thus, it is possible to divide ITBs into two types, so-called weak and so-called strong ITBs. The weak ITBs tend to exhibit only partial turbulence suppression, the diffusion coefficients being above the neo-classical levels and the gradients of the plasma profiles are not very large. On the other hand, the strong ITBs exhibit full turbulence stabilisation, large gradients and neo-classical transport levels. Thus, the whole concept of the power threshold for ITBs is not at all as unambiguous as for H-modes. In fact, the ITB formation seems to be more linked to the physical processes rather than the variations in power [51].

Simple models, like the Bohm/gyroBohm model, are of bifurcative nature (Heaviside step function used) and always assume full (or no) turbulence stabilisation. As the experimental evidence points towards a much more complicated picture, having possibly a two-step process, sometime with a bifurcative and sometime with a continuous transition, it is extremely challenging, if not impossible, to predict the time evolution of the strength and location of the ITB, as well as the plasma profiles within a good quantitative accuracy. To reach even a qualitative agreement might be challenging in many situations. The theory-based models, such as theWeiland model or GLF23 could in principle be able to predict a continuous process and both weak and strong ITBs. They can also predict ITBs only in one or a few transport channels simultaneously.

The interesting question to be raised now is how reliably we can predict the behaviour of the

ITB plasmas and develop the advanced tokamak scenarios with ITBs in future devices. The semiempirical Bohm/gyroBohm model seems to work fairly well in JET and in a similar size tokamak (JT-60U) and also to some extent in a smaller size tokamak (DIII-D) when including the -stabilisation. For ITER, assuming zero $\omega_{E\times B}$ shearing rate, the Bohm/gyroBohm model predicts an ITB if the condition $s < 0.6\ a - 0.5$ is satisfied. However, in general there is no guarantee that the same prediction accuracy can be extrapolated to much larger size tokamaks. In fact, as the predictions for the plasma profiles with the Bohm/gyroBohm model were poorer in a smaller size DIII-D than in similar sizes JET and JT-60U, the general problem with semi-empirical transport models was demonstrated – the uncertainties in the scaling with the size of the tokamak may be significant.

On the other hand, the time-dependent predictions for the ITB dynamics with the first-principle transport models, GLF23 and in particular the Weiland, are not in a satisfactory quantitative agreement with the experimental results from the present tokamaks. As a consequence, the timedependent, fully predictive results predicted with these models in ITB plasma scenarios in ITER cannot be regarded as reliable enough for the time being. This is a real problem for the development of advanced tokamak scenarios for ITER, where a proper alignment between the ITB and noninductive current is critical for steady-state operation [56]. Whether this alignment can be reached or not, depends strongly on the coupling mechanisms between the pressure and current profiles, which further depends strongly on ITBs. Therefore, future efforts must be further directed towards clarifying the role of different stabilisation mechanisms ($\omega_{E\times B}$ shearing rate, magnetic shear, α-stabilisation, role of rational q surfaces, ...), as well as understanding the triggering mechanisms and the magnitude of turbulence suppression within the ITB. In fact, similar efforts are needed in view of obtaining a good predictive capability for the H-mode pedestal or the edge transport barrier, as it plays an important role for the achievable fusion performance and current profile also in ITB scenarios. And finally that physics should be implemented into a reliable first-principle transport model, in view of developing advanced tokamak scenarios for steady-state operation in ITER.

ACKNOWLEDGEMENTS

This work has been conducted under the European Fusion Development Agreement. The authors are grateful to the ITPA Topical Group on Transport Physics for initialising this study and giving access to the ITPA ITB database. The authors also like to thank Jon Kinsey for his advice on using the GLF23 transport model and for the careful benchmark work of GLF23 between CRONOS and XPTOR transport codes. The authors also like to thank Clive Challis for many fruitful discussions during the work.

REFERENCES

[1]. Connor J.W, Fukuda T, Garbet X, Gormezano C et al. 2004 Nucl. Fusion **44** R1.

[2]. Connor J.W, Garbet X, Rogister A L, RomanelliMand Ryter F 2005 Plasma Phys. Control. Fusion **47** 941.

[3]. Connor J.W, Garbet X, Giannone L, Greenwald M. et al. 2003 Plasma Phys. Control. Fusion **45** 455.
[4]. Kinsey J.E., Staebler G.M and Waltz R.E. 2005 Phys. Plasmas **12** 052503.
[5]. Zhu P, Bateman G, Kritz A.H. and Horton W. 2000 Phys. Plasmas **7** 2898.
[6]. Gohil P, Kinsey J, Parail V, Litaudon X et al. 2003 Nucl. Fusion **43** 708.
[7]. Parail V, Baranov Y, Challis C, Cottrell G et al. 1999 Nucl. Fusion **39** 429.
[8]. Fukuda T and the International ITB database working group 2001 Proc. 28th European Physical Society Conf. on Controlled Fusion and Plasma Physics (Madeira, Portugal, 18{22 June, 2001) (ECA vol 25A), P-5.115.
[9]. Waltz R.E., Kerber D, Milovich J and Hammett G.W. 1995 Phys. Plasmas **2** 2408.
[10]. Waltz R.E., Kerber D and Milovich J 1994 Phys. Plasmas **1** 2229.
[11]. Waltz R.E., Staebler G.W., Dorland W, Hammett G.W. et al. 1997 Phys. Plasmas **4** 2482.
[12]. Hahm T.S. and Burrell K.H. 1995 Phys. Plasmas **2** 1648.
[13]. Burrell K.H. 1997 Phys. Plasmas **4** 1499.
[14]. Tala T.J.J, Heikkinen J.A, Parail V.V, Baranov Yu F and Karttunen S J 2001 Plasma Phys. Control. Fusion **43** 507.
[15]. Shirai H. 2000 Plasma Phys. Control. Fusion **42** A109.
[16]. Gohil P, Baylor L.R, Burrell K.H, Casper T.A. et al. 2003 Plasma Phys. Control. Fusion **45** 601.
[17]. Levinton F.M, Zarnstorff M.C, Batha S.H, Bell M et al. 1995 Phys. Rev. Lett. **75** 4417.
[18]. Strait E.J, Lao L.L, Mauel M.E, Rice B.W et al. 1995 Phys. Rev. Lett. **75** 4421.
[19]. Beer M.A, Hammett G.W, Rewoldt G, Synakowski E.J. et al. 1997 Phys. Plasmas **4** 1792.
[20]. Staebler G.M.1998 Plasma Phys. Control. Fusion **40** 569.
[21]. Ide S, Suzuki T, Sakamoto Y, Takenaga H et al. 2002 Plasma Phys. Control. Fusion **44** A137.
[22]. Fukuyama A, Fuji Y, Itoh S-I, Yagi M. and Itoh K. 1996 Plasma Phys. Control. Fusion **38** 1319.
[23]. Bourdelle C, Hoang G, Litaudon X, Roach C and Tala T et al. 2005 Nucl. Fusion **45** 110.
[24]. Bourdelle C, Dorland W, Garbet X, Gohil P et al. 2003 Proc. 30th European Physical Society Conf. on Controlled Fusion and Plasma Physics (St. Petersburg, Russia, 7{11 July, 2003) (ECA vol 27A), P-1.89.
[25]. Staebler G M 1999 Nucl. Fusion 39 815.
[26]. Tala T J J, Parail V V, Becoulet A, Corrigan G et al. 2002 Plasma Phys. Control. Fusion **44** A495.
[27]. Joffrin E, Challis C D, Hender T C, Howell D F, Huysmans G T A 2002 Nucl. Fusion **42** 235.
[28]. Garbet X 2001 Plasma Phys. Control. Fusion **43** A251.
[29]. Erba M, Cherubini A, Parail V V, Springmann E and Taroni A 1997 Plasma Phys. Control. Fusion **39** 261.
[30]. Weiland J "Collective Modes in Inhomogeneous Plasma" Institute of Physics Publishing, Bristol 2000.
[31]. Strand P, Nordman H, Weiland J and Christiansen J 1998 Nucl. Fusion **38** 545.

[32]. Waltz R.E. and Miller R .1999 Phys. Plasmas **6** 4265.
[33]. Bourdelle C, Garbet X, Hoang T, Ongena J. and Budny R. 2002 Nucl. Fusion **42** 892.
[34]. Basiuk V, Artaud J F, Imbeaux F, Litaudon X. et al. 2003 Nucl. Fusion **43** 822.
[35]. HoulbergW.A, Shaing K.C, Hirschman S.P. and Zarnstorff M.C. 1997 Phys. Plasmas **4** 3230.
[36]. Genacchi G, and Taroni A. 1988 JETTO: A free boundary plasma transport code (basic version), Rapporto ENEA RT/TIB 1988(5).
[37] Maget P, Esposito B, Joffrin E, Hawkes N. et al. 2003 Plasma Phys. Control. Fusion **45** 1385.
[38]. Ohkawa T 1978 Phys. Lett. A **67** 35.
[39]. de Esch H P L, Stork D and Weisen H 1990 (Proc. 17th European Physical Society Conf. on Controlled Fusion and Plasma Physics (Amsterdam, The Netherlands, 25{29 June, 1990) (ECA vol 14B) p 90.
[40]. Maget P, Xarbet G, Geraud A. and Joffrin E. 1999 Nucl. Fusion **39** 949.
[41]. Jarmen A, Andersson P and Weiland J 1987 Nucl. Fusion **27** 941.
[42]. Nordman H, Weiland J and Jarmen A 1990 Nucl. Fusion **30** 983.
[43]. Weiland J and Hirose A 1992 Nucl. Fusion **32** 151.
[44]. Huysmans G.T.A 1991 CP90 Conf. on Comp. Physics, World Scientific p. 371.
[45]. Kinsey J.E, Staebler G.M. and Waltz R.E. 2002 Phys. Plasmas **9** 1676.
[46]. Weiland J. and Holod I. 2005 Phys. Plasmas **12** 012505.
[47]. Baranov Yu F, Garbet X, Hawkes N C, Alper B et al. 2004 Plasma Phys. Control. Fusion **46** 1181.
[48]. Tardini G, Peeters A G, Pereverzev G V and Ryter F 2002 Nucl. Fusion **42** 258.
[49]. Dimits A.M, Bateman G, Beer M.A, Cohen I et al. 2000 Phys. Plasmas **7** 969.
[50]. Mantica P, Van Eester D, Garbet X, Imbeaux F 2005 “New evidence on Internal Transport Barrier physics from heat pulse propagation experiments”, submitted to Phys. Rev. Lett.
[51]. Challis C D, Litaudon X, Tresset G, Baranov Yu F et al. 2002 Plasma Phys. Control. Fusion **44** 1031.
[52]. Koide Y, Kikuchi M, Mori M, Tsuji S. et al. 1994 Phys. Rev. Lett. **72** 3662.
[53]. Greenfield C.M, Rettig C.M, Staebler G.M, Stallard B.W. et al. 1999 Nucl. Fusion **39** 1723.
[54]. Lopes Cardozo N.J, Hogeweij G.M.D, de Baar M, Barth C.J. et al. 1997 Plasma Phys. Control. Fusion **39** B303.
[55]. Fitzpatrick R, Hastie R.J, Martin T.J and Roach C.J. 1993 Nucl. Fusion **33** 1533.
[56]. Taylor T.S. 1997 Plasma Phys. Control. Fusion **39** B47.

Tokamak	Pulse No:	Bϕ (T)	I_p (MA)	P_{in} (MW)	Reversed q
JET	46664	3.4	3.4	22	no
JET	53521	3.4	2.0	22	yes
JT-60U	34487	3.7	1.5	13	no
JT-60U	39056	3.7	1.3	8	yes
DIII-D	87031	2.1	1.6	9	no
DIII-D	95989	2.1	1.6	5	yes

Table 1: The simulated discharges from the ITPA ITB database.

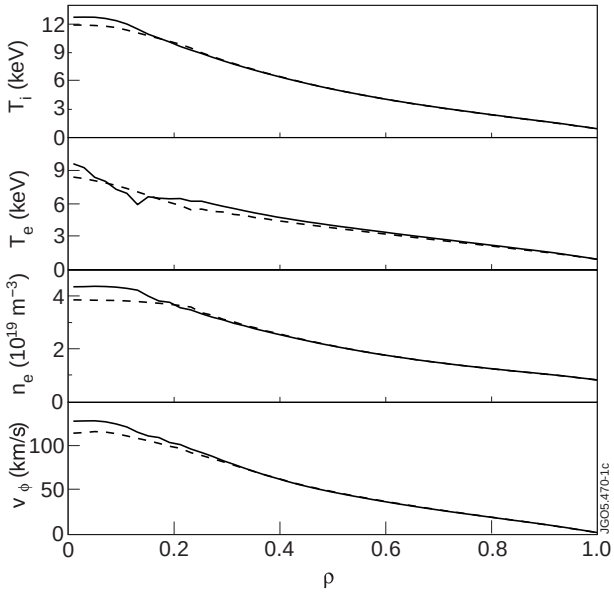

Figure 1: The ion and electron temperature, density and toroidal rotation velocity profiles for JET Pulse No: 46664 at t = 6.0s, after 3s simulation from the preheating phase towards an ITB phase. The dashed lines correspond to the simulation with the Weiland model including 10% of additional Bohm transport and the solid lines are from the simulation without it.

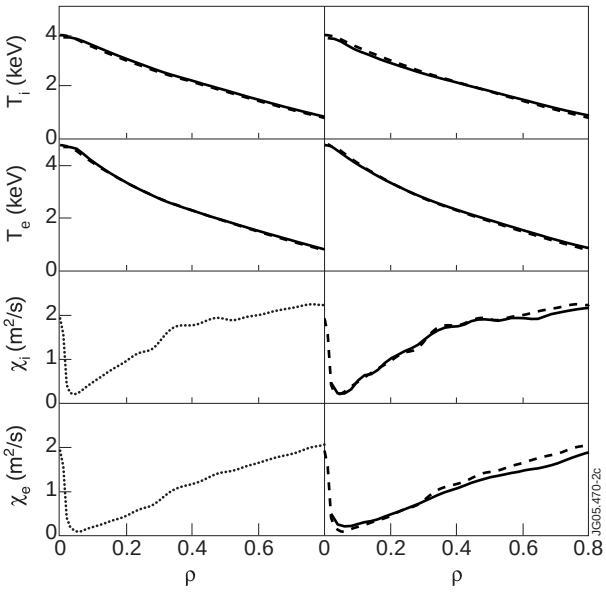

Figure 2: The ion and electron temperature, and the ion and electron diffusion coefficients for a simple L-mode benchmark case (based on the JET Pulse No: 52009 at t = 16.0s) with the same i and e (left frame) and using the GLF23 transport model (right frame). The dashed lines correspond to the simulation with cronos code and the solid lines with jetto code (the dotted lines are common for both the codes).

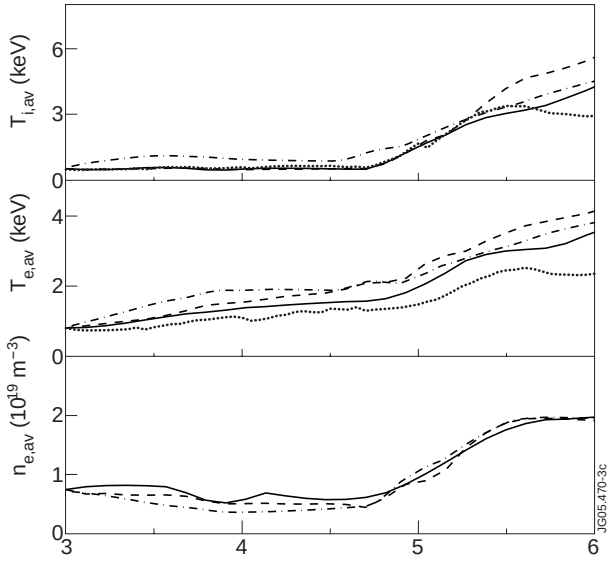

Figure 3: Time traces of the volume averaged ion temperature, electron temperature and electron density for JET Pulse No: 46664. The solid lines correspond to the experimental data and the dashed, dashdotted and dotted lines to the predictions by the Bohm/GyroBohm, Weiland and GLF23 transport models, respectively.

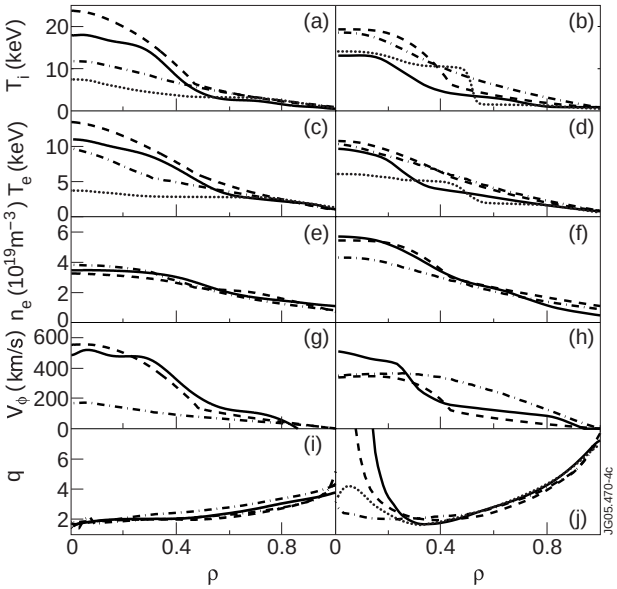

Figure 4: Profiles of the ion temperature (a) and (b), electron temperature (c) and (d), electron density (e) and (f), toroidal rotation (g) and (h) and q (i) and (j) for JET Pulse No: 46664 at t=6.0 s (left-hand side) and 53521 at t=12.0 s (right-hand side). The solid lines correspond to the experimental data and the dashed, dash-dotted and dotted ones to the predictions with the Bohm/GyroBohm, Weiland and GLF23 transport models, respectively.

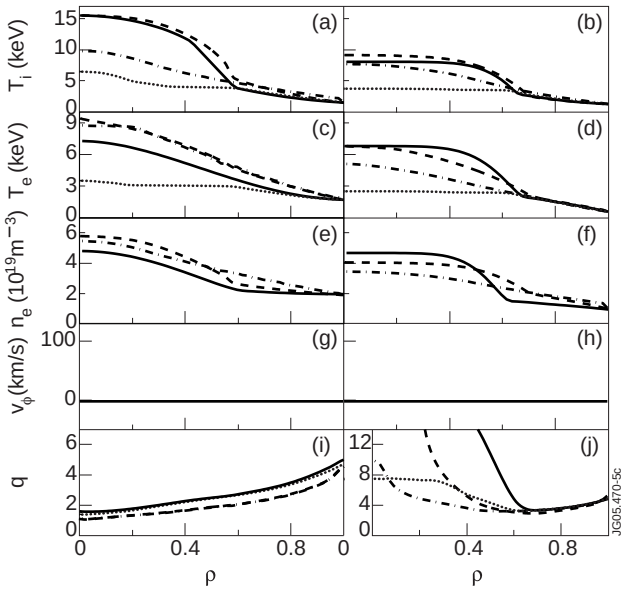

Figure 5: As in figure 4, but for JT-60U Pulse No's: 34487 at t=5.0s (left-hand side) and 39056 at t=6.8s (right-hand side).

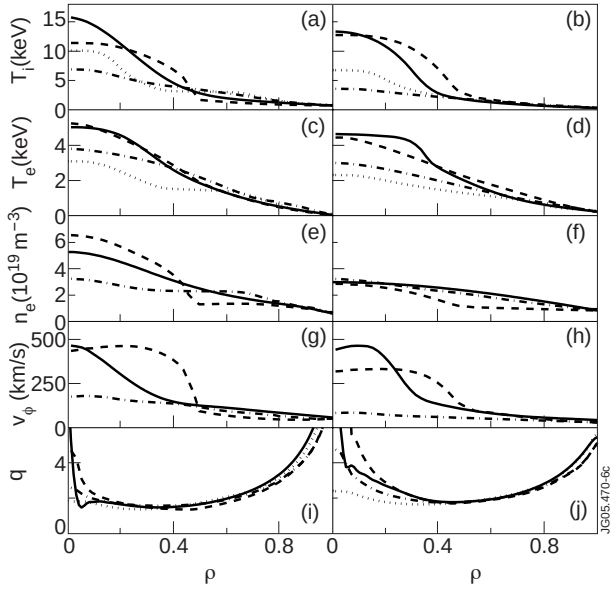

Figure 6: As in figure 4, but for DIII-D Pulse No's: 87031 at t=1.85s (left-hand side) and 95989 at t=0.95s (right-hand side).

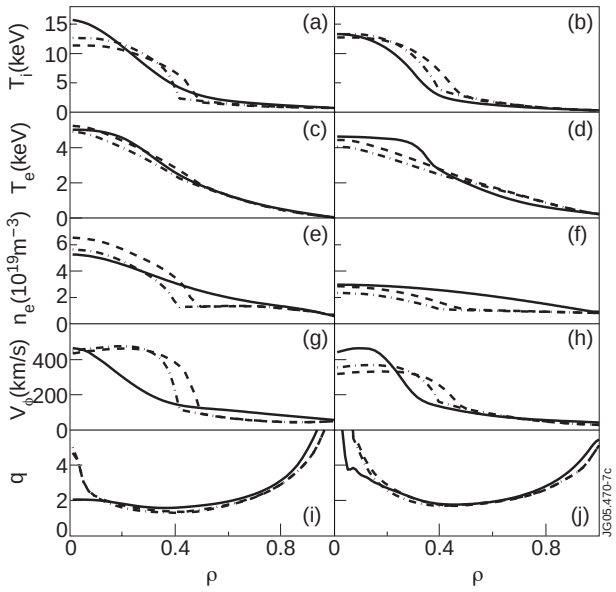

Figure 7: As in figure 6 for the two DIII-D discharges (solid is the experiment and dashed the prediction by the Bohm/GyroBohm model), but now the dash-dotted lines correspond to the predictions with the amended ITB model including the α-stabilisation.

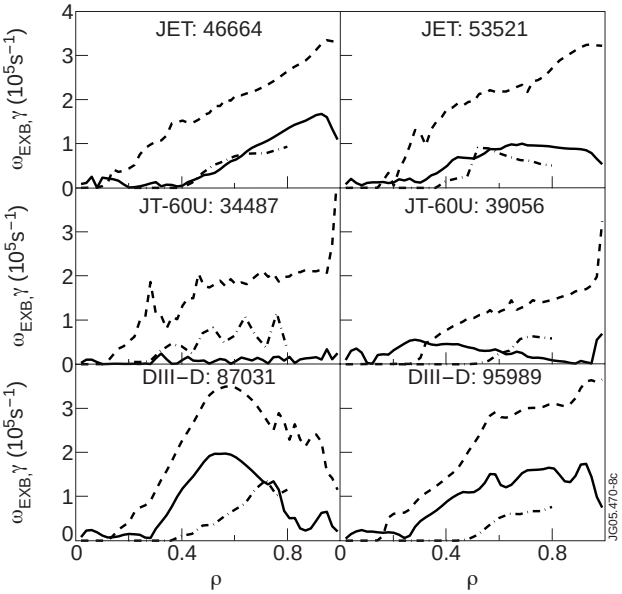

Figure 8: The ω_{ExB} shearing rates (solid lines) and the linear growth rates (dashed lines) calculated by the Weiland model for JET Pulse No's:46664 and 53521, JT-60U Pulse No's: 34487 and 39056 and DIII-D Pulse No: 87031 and 95989. The dash-dotted lines present the growth rates calculated with kinezero. The times of the micro-stability analysis correspond to those in figures 4–6 for each discharge, respectively.

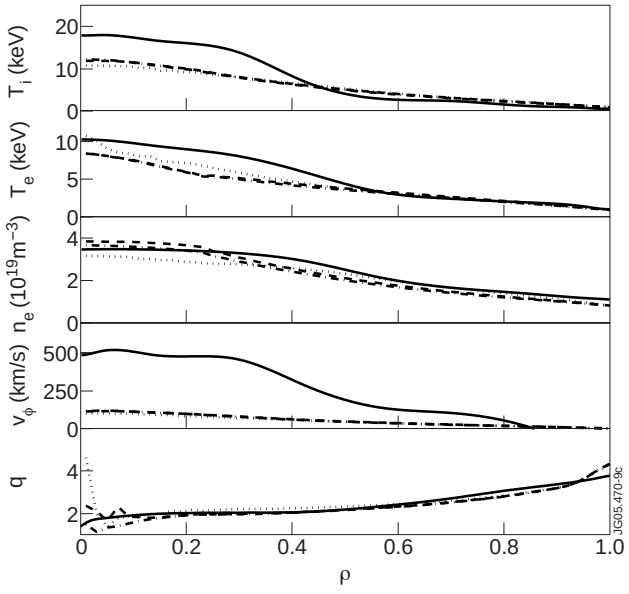

Figure 9: The simulation predictions with the different versions of the Weiland model for JET Pulse No: 46664 at t = 6.0s. The solid lines correspond to the experimental data and dashed, dotted and dash-dotted lines the simulations with the standard version, with EM effects and collisions switched on and with the model with the variable correlation length, respectively.

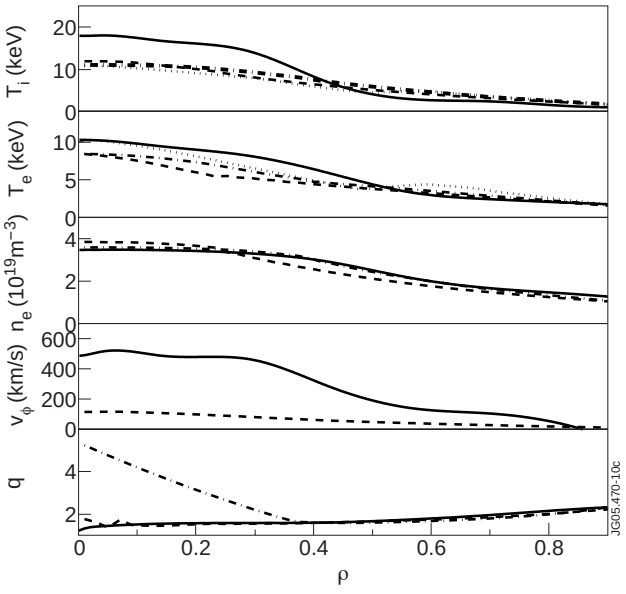

Figure 10: The simulation predictions employing layered tests with the Weiland model for JET Pulse No: 46664 at t = 6.0s. The solid lines correspond to the experimental data and dashed, dotted and dash-dotted lines the simulations with the standard version, with fixing T_i, T_e and ne to their experimental values and with a fixed, strongly reversed q, supplemented with the experimental v_ϕ, respectively.

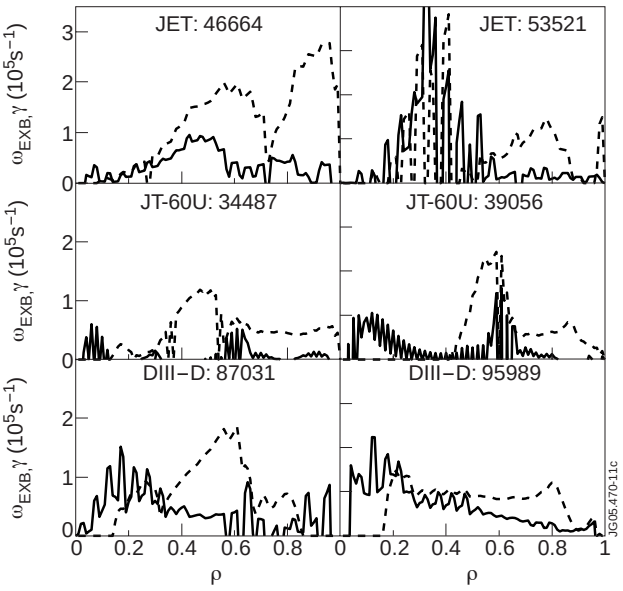

Figure 11: The ω_{ExB} shearing rates (solid lines) and the linear growth rates of the fastest growing mode (dashed lines) calculated by the GLF23 model for JET Pulse No's: 46664 (a) and 53521 (b) and DIII-D Pulse No's: 87031 (c) and 95989 (d). The times of the micro-stability analysis correspond to those in figures 4 – 6 for each discharge, respectively.